Biosensors and Bioelectronics 142 (2019) 111505

Contents lists available at ScienceDirect

Biosensors and Bioelectronics

journal homepage: www.elsevier.com/locate/bios

Current status of optical fiber biosensor based on surface plasmon resonance

Yong Zhao[a,b,*], Rui-jie Tong[b], Feng Xia[b], Yun Peng[b]

[a] State Key Laboratory of Synthetical Automation for Process Industries, Shenyang, 110819, China
[b] College of Information Science and Engineering, Northeastern University, Shenyang, 110819, China

ARTICLE INFO

Keywords:
Surface plasmon resonance
Biosensor
Optical fiber biosensor
Optical fiber grating

ABSTRACT

Surface plasmon resonance (SPR) technology has effectively bolstered optic fiber sensing in fields of life science, clinical diagnosis, medicine, food safety and so on. The current review outlines the research status of fiber optic biosensor based on SPR, and the merits of optical fiber sensor and the development of optical fiber sensor based on SPR are completely covered. An in-depth review of four devices for generating SPR is presented, and optical fiber is finally adopted for a substrate to generate SPR. Different prototypes of optical fiber biosensor based on SPR are meticulously outlined: optical fiber grating biosensor based on SPR and optical fiber structured type biosensor based on SPR, and representative instances from literature are presented to verify the latest advancements in this potentially valuable research avenue. In addition, the sensing performance of different optical fiber structured type biosensor based on SPR are compared. What's more, simultaneous multi-parameter detection and improvement of sensitivity are discussed and summarized. The article concludes identify key challenges and develop orientation of optical fiber biosensor based on SPR.

1. Introduction

Real-time monitoring of living cells (Zhang, Y. et al., 2016), proteins (Tu et al., 2018; Xu et al., 2019), toxins, viruses (Ji et al., 2016), bacteria, glucose, and various chemical gas (Wang, H. Z. et al., 2019) is significant in food hygiene (Zainuddin et al., 2018; Srivastava et al., 2012), cytobiology (Shi et al., 2016), microbiological detection (SlaviK et al., 2002), pharmaceutical research and development (Perlette and Tan, 2001), and so on (Updike and Hicks, 1967; Wang, M. et al., 2018; Boruah and Biswas, 2018). In 1967, Updike and Hicks proposed the first biosensor (An et al., 2014). At present, there are many methods for bio-sensing, such as optical, electro-chemical, thermometric, piezoelectric or magnetic. Among them, optical fiber biosensor based on SPR are the most accepted by researchers which exhibit impressed commercial value in chemistry, life sciences and other fields (Liu et al., 2013; Shrivastav et al., 2015). In 1983, Liedberg proposed the first sensor based on SPR (Liedberg et al., 1983). However, traditional prism sensors based on SPR suffer from bulky sensing device, which limits the practical application in point-to-point detection (Sergiy et al., 2003; Dai et al., 2018). But optical fiber sensor possesses great advantages, such as small bulk (Yong et al., 2018a), light weight (Zhang, Y. N. et al., 2018), anti-electromagnetic interference (Yong et al., 2018b), long distance transmission (Yu et al., 2018), in situ monitoring (Ruijie et al., 2018) and so on, which have attracted much attention in bio-sensing. In 1996, Kao studied the transmission characteristics and loss of light quartz optical fibers in detail (Kao and Hockham, 1966), and proved the possibility of making low loss optical fibers in theory. In 1970, Corning Corporation of the United States successfully developed the word's first low-loss quartz optical fiber, which proved the practicability of optical fiber as a medium of light transmission (Jorgenson and Yee, 1993). In 1993, Jorgenson first proposed the fiber optic probe based on SPR (Jorgenson, 1993). Objectively speaking, due to various sensing structure of optical fiber, optical fiber biosensor based on SPR has attract much attention and achieved satisfactory results (Lee et al., 2009; Caucheteur et al., 2015; Gupta and Kant, 2018).

The current review presents a supremely distinguished and hugely promising research avenue of optical fiber biosensor based on SPR. Different devices for generating SPR are systematically introduced and optical fiber coupling prototype is adopted for optical fiber biosensor based on SPR. Different geometrical of fabricating optical fiber sensing probe and corresponding sensing principle are in-depth discussed, and instances are provided to verify feasibility of proposed plan. In addition, detection of multiple parameters and improvement of sensitivity are meticulously studied. Finally, key challenges and develop orientation of optical fiber biosensor based on SPR are identifying.

* Corresponding author. State Key Laboratory of Synthetical Automation for Process Industries, Shenyang, 110819, China.
E-mail address: zhaoyong@ise.neu.edu.cn (Y. Zhao).

https://doi.org/10.1016/j.bios.2019.111505
Received 2 June 2019; Accepted 12 July 2019
Available online 16 July 2019
0956-5663/

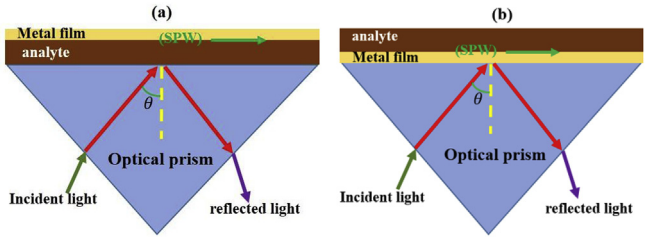

Fig. 1. (a) Otto configuration, (b) Kretschmann configuration.

2. SPR sensing configuration

SPR is generated by the excitation of surface plasmon polaritons, which is generated by the combination of free electron density oscillations and electromagnetic waves on the surface between dielectric medium and metal film. Surface plasmon wave or surface plasmon polaritons is another form of SPR, and belongs to transverse magnetic or p-polarized light wave that is a vector wave perpendicular to the incident plane and propagates along the upper surface of metal film (Guo, 2012). According to different excitation model, the types of SPR sensors are prism coupled sensor, waveguide coupled sensor, grating coupled sensor, and optical fiber coupled sensor.

2.1. Prism coupling

In 1950s, Ritchie theoretically introduced surface plasmons in detail (Ritchie, 1957). In 1968, Otto studied prism coupled SPR with Otto configuration, which was based on attenuated total reflection (Otto, 1968). The sensing configuration is shown in Fig. 1(a), the analyte separates the prism and plasmonic metal layer, which makes the sensing device complex (Kretschmann and Raether, 1968; Kretschmann, 1971). And then, Kretschmann upgrades the Otto configuration that can be seen in Fig. 1 (b), where the metal film is between prism analyte, and the resonance condition can be described as (Schasfoort and Tudos, 2008):

$$k_{sp} = \frac{w}{c}\left(\frac{\varepsilon_m \varepsilon_d}{\varepsilon_m + \varepsilon_d}\right) = k_d = \frac{w}{c}\sqrt{\varepsilon_p}\sin\theta \tag{1}$$

Where c is defined as the speed of light propagation in vacuum, ε_d and ε_m present dielectric constants of dielectric and metal film, respectively, w is the angular frequency. k_{sp} is propagation constant of surface plasmon, θ represents the incident angle, and k_d is propagation constant of evanescent wave that can be given by:

$$k_d = \frac{w}{c}\sqrt{\varepsilon_p}\sin\theta \tag{2}$$

The free electrons will resonate when the frequencies of incident electros and surface electrons are same, and propagates along the metal-dielectric interface.

Kretschmann and Otto configurations have been already mature for SPR sensing, however, the sensor structure is large, the sensor system is complex and the manufacture is troublesome, which isn't conducive to remote monitoring.

2.2. Waveguide coupling

The sensing device is shown in Fig. 2, where the light propagate is depends on total internal reflection. When the light transmits in the waveguide coupling device, partially transmitted light exists in the form of evanescent wave. In the case of resonance condition, evanescent wave passing through metal film, which will be affected by analyte (Wijaya et al., 2011). The principle of SPR generation in waveguide device is the same as that in prism device, the only difference is the configuration.

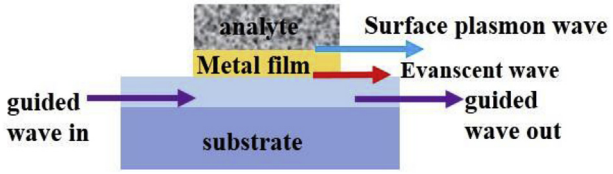

Fig. 2. Optical waveguide coupling device.

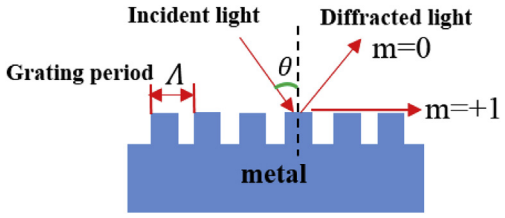

Fig. 3. Surface plasmon device by grating coupling.

2.3. Grating coupling

By inserting diffraction grating in sensing structure, the momentum of incident optic wave will be enhanced, and the diagram of grating coupled sensor is presented in Fig. 3. When incident light travels to the metal dielectric interface at an angle of θ (the resonant angle), diffraction occurred in grating coupler can also enhance the energy of incident light wave. The original x-component of wave vector of incident photons k_x can be improved by G and m= 0, ±1, ±2..., where G is wave number of grating, and m is diffraction order.

The resonance condition is realized by m. Coupling condition can be expressed by Eq. (3), where k_d presents a constant value of diffracted light, Λ is period of grating device, and n_d represents the dielectric refractive index (Wijaya et al., 2011).

$$k_d = k_x + mG = \frac{2\pi}{\lambda} n_d \sin\theta + m\frac{2\pi}{\Lambda} \tag{3}$$

Therefore, the propagation constant (k_d) of the diffraction grating can be expressed by integer multiple of the wavenumber of grating (G).

2.4. Optical fiber coupling

The large bulk of prism type, optical waveguide type and metal grating type limit their application in narrow and long-distance measurement. Optical fiber coupling has drawn researchers' attention due to its compact structure that enables it applied in narrow space, real time detection, and even in-situ measurement in vivo. For standard optic fiber, the evanescent field is almost zero in cladding of optical fiber, which can't excite SPR. In order to generate SPR, three conditions need to be satisfied simultaneously: firstly, part of the energy in fiber core leaks into fiber cladding. Secondly, the thickness of the metal coating should be moderate, generally speaking, the thickness is 30–50 nm. Thirdly, polarization state of the cladding mode should be controlled.

After the first optical fiber sensor based on SPR proposed, Liedberg first applied SPR technology in biochemical detection (Liedberg et al., 1993). The change of biomass will affect refractive index on the surface of sensing structure, so as to realize the measurement of biomass (Sharma et al., 2007; Mishra et al., 2015; Srivastava et al., 2016).

After 25 years of development, the fiber optic sensing technology based on SPR has been quite mature. At present, there are two types of optical fiber biosensor based on SPR: optical fiber grating biosensor based on SPR and optical fiber structured type biosensor based on SPR. In the following chapters of this review, optical fiber grating biosensor based on SPR and the optical fiber structured type biosensor based on SPR are introduced, respectively.

3. Prototype and sensing mechanism of optical fiber sensor based on SPR

Optical fiber sensors are multitudinous, considering the condition of optical fiber core, optical fiber sensors based on SPR are divided into two types: optical fiber grating biosensor based on SPR and optical fiber structured type biosensors based on SPR. The clad of optical fiber grating is intact, while that of optical fiber structured type biosensor is worked. The most important is that the sensing principle is disparate.

3.1. Optical fiber grating biosensor based on SPR

Fiber grating, a kind of fiber device with permanent period change of refractive index on the fiber core, can be made by laser lithography technology, and Hill made an optical fiber grating with germanium doped by standing wave writing for the first time in 1978 (Hill et al., 2008). After forty years of development, the fabrication of optical fiber grating has been mature and commercialized, and they can divided into two categories: long period fiber grating and short period fiber grating. Optical fiber grating not only has the advantages of small size, anti-electromagnetic interference and anti-corrosion, but also can realize distributed measurement (Weis et al., 1994; Zhang, J. et al., 2009; Luo et al., 2015; Yong et al., 2019). Therefore, the combination of optical fiber grating and SPR to measure biomass has become a hot research topic and achieved good results (Shevchenko et al., 2011; Valérie et al., 2014; Guo et al., 2016a). In this chapter, optical fiber grating biosensor based on SPR are introduced according to grating period classification.

3.1.1. Short period optical fiber grating biosensor based on SPR

Short period fiber grating refers to its grating period less than 1 μm, and short period optical fiber grating can be divided to fiber Bragg grating (FBG) and tilted fiber Bragg grating (TFBG) by relationship between refractive index modulation direction and fiber axis. Fig. 4 is the diagram of FBG and TFBG. For FBG, direction of the refractive index modulation is perpendicular to the axis of fiber. While, the refractive index modulation direction of the TFBG and the fiber axis form a certain angle and the angle is less than 45.

In 1989, Meltz fabricated a FBG by ultraviolet laser (Meltz et al., 1989). After decades of development, FBG has been widely adopted for sensing (Kang et al., 2011; Wada et al., 2012), and the sensing principle can be described/as: effective refractive index, length and the grating period of FBG affect by the change of surrounding refractive index, which will change the grating resonance condition, and then the resonance wavelength changes. In addition, FBG has narrowband that is good for reading correct data and reducing experiment error.

According to phase matching condition, the central wavelength λ_B of FBG can be described as:

$$\lambda_B = 2n_{eff}\Lambda \tag{4}$$

Where n_{eff} is effective refractive index of FBG, and Λ is the periodicity of FBG. But for standard FBG, the coupling only happens between core modes that restrict the influence of external refractive index on the transmission of light in fiber core. In order to adopt FBGs for bio-sensing, the cladding of FBG must be reduced, and traditional methods are etched, grinded and fine-drawn cone (Lyons and Lee, 1999; Liu, X. et al., 2003; Iadicicco et al., 2004), after which, the transmitted light in fiber core will be influenced by external refractive index (Chryssis et al., 2005), and the resonance wavelength of cladding reduced FBG can be forecasted, and cladding etched FBGs can be adopted for biochemical molecules detection by coating corresponding material film on the surface of sensing region.

In 2016, Arasu proposed a sensor based SPR with gold film coated on the surface of FBG (Arasu et al., 2016), and graphene oxide film was coated on the surface of gold film with the thickness of 45 nm to enhance sensitivity of the proposed sensor. Experimental results revealed that the sensitivity of proposed sensor was up to 200 nm/RIU when it tested anhydrodus ethanol aqueous solution, which is 2.5 times higher than that without any GO film assisted, and repetitive experiment also presented good result.

Although anhydrodus ethanol aqueous solution was not biomass, this research revealed FBG had potential to be adopted for bio-sensing.

TFBG is first proposed by American scholar Meltz in 1990 (Meltz et al., 1990). Unlike FBG, the modulation direction is inclined to the axial direction of optic fiber, and the modulation period is generally ~500 nm (Sipe and Erdogan, 1996; Guo et al., 2016b). As shown in Fig. 4 (b), TFBG has the ability to couple the transmit light into backward cladding. On the left hand side of the Bragg resonance which corresponds to the core mode self-coupling, the amplitude of transmitted spectrum presents dozens of narrow-band cladding mode resonances (FWHM ~200 p.m. or even below). According to weak waveguide approximate electromagnetic theory, the relationship between effective refractive index of each cladding mode and its coupling wavelength can be expressed:

$$\lambda_{clad,i} = (n_{clad,i} + n_{core})\Lambda/\cos\theta \tag{5}$$

Where i represents modulus, n_{core} and $n_{clad,i}$ are effective refractive index of fiber core and i order cladding mode, respectively. θ is the angle between the grid and the axial normal line of the optical fiber.

According to phase matching condition, the maximum sensitivity will be obtained when effective index of corresponding cladding modes is similar to surrounding refractive index. In 2001, Laffont first applied TFBG for surrounding refractive index sensing (Laffont and Ferdinand, 2001), and then, Prof. Jacques Albert (working Carleton University of Ottawa) first proposed TFBG sensor based on SPR (Shevchenko and Albert, 2007). TFBG sensor based on SPR makes the detection of biological molecules become true by depositing biological molecules on the surface of active golden film. Up to now, there have been a few reports about TFBG sensors based on SPR for cells sensing. There are not only transmission TFBG sensors based on SPR, but also reflective TFBG sensors based on SPR made by coating mirrors at the end of grating, which is more suitable for narrow measurement environment.

In 2017, Zhang, Y. proposed a neoteric label free TFBG biosensor based on SPR for glycoprotein measurement (Zhang, Y. et al., 2017). In the sensing diagram, a 10° TFBG coated with a thickness of 50 nm Au film was adopted for SPR inspiring, the sensing probe was shown in Fig. 5. Phenylboronic acid was immobilized on the sensing probe as glycoprotein recognition molecule, the process was shown in Fig. 6: the proposed sensor was cleaned by dipping into boronic acid derivative for 24 h, and then, molecules were transferred on the surface of the TFBG sensor by self-assemble with. Finally, Con A solution with different concentration (0.02, 0.1, 0.25, 0.5, and 1 mg/mL) were tested. Experiment results shown in Fig. 7 indicates that the amplitude decreased as the concentrations increased.

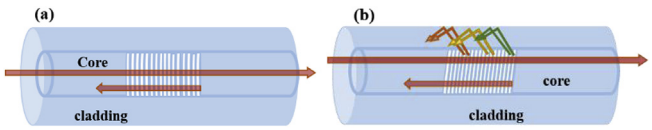

Fig. 4. (a) Sketch of the FBG, (b) sketch of the titled FBG.

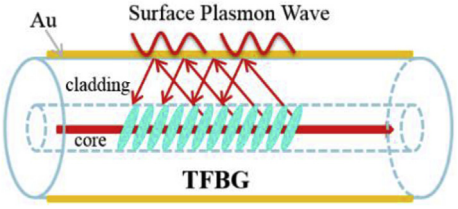

Fig. 5. Sensing structure of TFBG biosensor based on SPR (Zhang, Y., 2017).

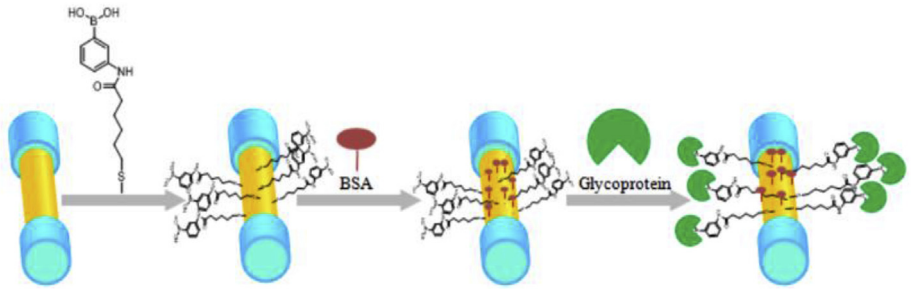

Fig. 6. The process of the protein immobilization and protein specific identification (Zhang, Y., 2017).

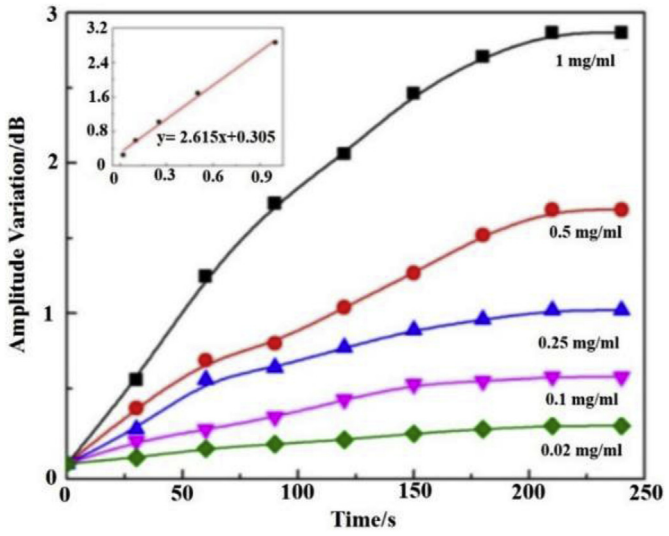

Fig. 7. Experiment results with different concentration of Con A (Zhang, Y., 2017).

The inset in Fig. 7 presented the linear relationship between amplitude and the concentrations of sample. The sensitivity of protein was 2.857 dB/(mg/mL), and the detection LOD of protein was 15.56 nM, the results were calculated by the IUPAC criteria (3σ/M). Considering the advantages of the proposed sensor process, such as temperature insensitive, compact size, good commercial prospects and so on, the proposed sensor has the potential to be adopted for cell-to-cell interaction and recognition between biological molecules.

In 2018, Hu proposed a sensor with gold film coated on surface of TFBG, and then, covered a layer of graphene to surface functionalization (Hu et al., 2018), which was shown in Fig. 8.

After capturing dopamine molecules by aptamer molecules of DNA, the macromolecular ssDNAs occurred, and the refractive index around surface of optical fiber changed. Experiment results indicated that the LOD of proposed sensor was 1.6×10^{-13} M with concentration between 10^{-13} M and 10^{-8} M. What's more, accurate on-line measurement of dopamine with sub-microliter volumes could be realized by combination of microfluidic channels with TFBG biosensor based on SPR. At the same time, the aptamer for dopamine could be replaced by other aptamer and corresponding molecules can be measured by proposed sensor.

3.1.2. LPFG biosensor based on SPR

In 1996, Vengsarkar fabricated the first LPFG by amplitude mask method using ultraviolet laser on Ge-doped fiber (Vengsarkar et al., 1996b). Unlike short period fiber grating, the refractive index modulation period of LPFG is generally in tens to hundreds of microns (Vengsarkar et al., 1996a; Bhatia and Vengsarkar, 1996). Fig. 9 is the diagram of LPFG, which indicates the transmission direction of core and cladding are the same.

There is no backward emission in LPFG, which means LPFG can act as a transmission band stop filter. The spectrum of LPFG is composed by a number of resonant peaks, which is larger than 20 nm and distributed in the wavelength range of several hundred nanometers. According to the theory of light-wave coupling film, the position of resonance peaks correspond to the effective refractive index of fiber core and cladding can be described as:

$$\lambda_{clad,i} = (n_{core} - n_{clad,i})\Lambda \quad (6)$$

Eq. (6) indicates that $\lambda_{clad,i}$ depends on the difference of refractive index in fiber core and cladding. In addition, $n_{clad,i}$ is affected by surrounding refractive index. Therefore, LPFG can be adopted for sensing. At the same time, LPFG has low insertion loss and small backward reflection.

For LPFG, transmit light can couple the core mode into cladding mode and surface plasmon polaritons (Heather et al., 1998; Chong et al., 2004; Tsuda and Urabe, 2009), hence, the spectrum of transmission light will be attenuation, and experiments have been verified that the sensitivity can be improved by combination of LPFG and SPR (Patrick et al., 1998). During the past decades, biosensor and chemosensors based on LPFG with metal material covered have stepped into

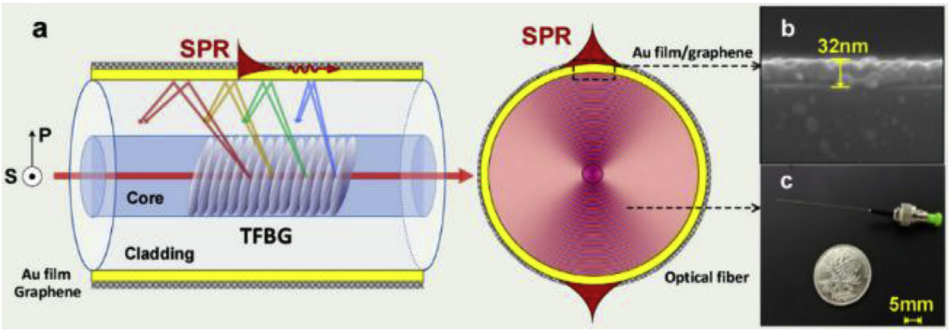

Fig. 8. (a) Optic fiber sensing structure with gold film cover on TFBG; (b) SEM image of gold film covered on the surface of TFBG; (c) photograph of proposed sensor (Hu et al., 2018). (For interpretation of the references to colour in this figure legend, the reader is referred to the Web version of this article.)

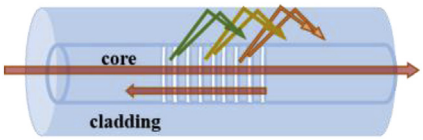

Fig. 9. Structural and light propagation direction of LPFG.

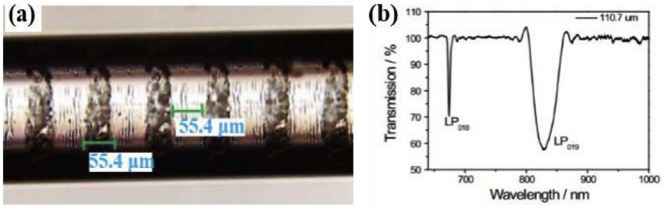

Fig. 10. (a) Microscopic image of the LP23FG; (b) transmission spectrum of the LPFG (Marques et al., 2016).

people's horizon.

In 2016, L. Marques proposed a biosensor with (PAH/SiO_2: Au NPs)$_3$ film coated on the surface of LPFG for streptavidin protein sensing (Marques et al., 2016). The diagram of adopted LPFG was shown in Fig. 10, where the length and grating period were 40 mm and 110.7 μm, respectively.

In order to realize the measurement of specific biomass, corresponding nanoparticles should be transferred on surface of LPFG, and the process were shown in Fig. 11. Experiment results were shown in Fig. 12.

In order to avoid the influence of solution volume on measurement, the sensing region should be washed and dried after each measurement. Experimental operation process was executed at 23 °C and 50 %RH. Finally, the sensitivity and theoretical LOD were 6.88 nm/(ng/mm)^2 and 19 pg/mm^2.

3.2. Optical fiber structured type biosensor based on SPR

Surface plasmon wave is, generated by external radiations, a transverse magnetic polarized electromagnetic wave, which propagates along the metal-dielectric and decays in exponential form. For a fiber optic covered with metal material, SPR effect can occur only part of light transmitted in fiber core leak out into fiber cladding. After decades of development, optical fiber biosensor based on SPR have been diffusely researched. In this part, according to the different optical fiber sensing structures, we introduce the fiber optic biosensor based on SPR in six types: hetero-core sensing structure, unclad/etched sensing structure, D-shaped sensing structure, tapered sensing structure, U-shaped sensing structure and end-face reflected sensing structure.

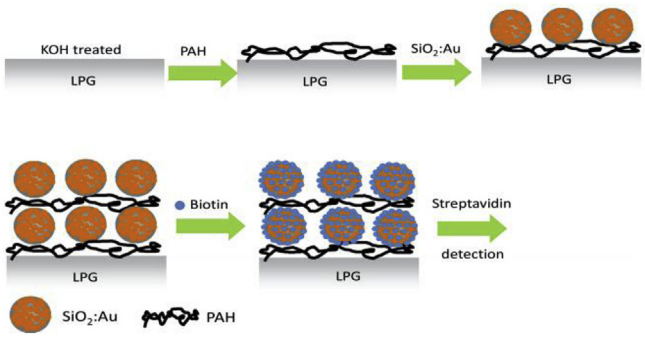

Fig. 11. Transferring process of (PAH/SiO_2: Au)$_2$ film on the surface of LPFG (Marques et al., 2016).

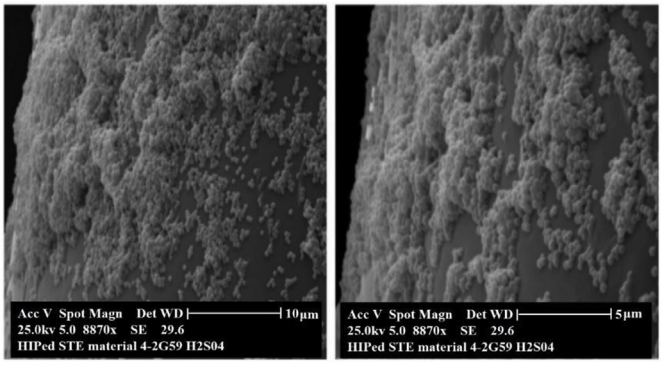

Fig. 12. SEM images of LPFG with (PAH/SiO_2 (300 nm):Au)$_3$ film covered (Marques et al., 2016).

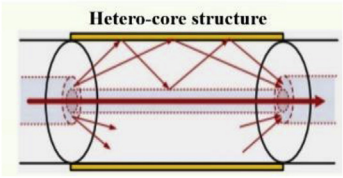

Fig. 13. The diagram of hetero-core structure (Hosoki et al., 2013).

3.2.1. Hetero-core sensing structure

Hetero-core structure, presented in Fig. 13, has been widely researched in recent years (Takagi et al., 2010; Wong et al., 2013; Hosoki et al., 2013; Liu et al., 2017), and the core diameter of inserted optical fiber should be smaller than that of two end optical fiber. When incident light transmitted to the first junction of two optical fiber, most of incident light leak out to clad of inserted optical fiber and form total internal reflection on surface of inserted optical fiber, and then evanescent wave occurs. After covering the surface of inserted fiber with metal material, the resonant wavelength subjects to external refractive index of inserted fiber. Therefore, the hetero-core structure sensor can realize measurement of refractive index. The inserted optical fiber of mismatched fiber-optic SPR sensor is mainly multimode fiber and photonic crystal fiber. In addition, inserting a segment of single-mode fiber between two segments of multimode fiber is also accepted.

In 2018, Qi Wang proposed a SPR sensor with SPA and graphene oxide co-covered on photonic crystal fiber (Qi and Botao, 2018a). The sensing structure was made by splicing a segment of photonic crystal fiber between two segments of multimode fiber. Gaphene oxide with large number of oxygen-containing functional had large specific surface area, which was advantageous to the contact between Au film and external medium, so as to improve the sensitivity of proposed sensor. Fig. 14 (a)-(c) detailed express the amination process on the surface of photonic crystal fiber, Fig. 14 (d) was the process transferring graphene oxide on surface aminated photonic crystal fiber. The combination of SPA and antibodies in Fc region was favorable to improve the degree of antibodies capture, and the capturing process was presented in Fig. 14 (e)-(g). Fig. 15 was the experimental results, which revealed that the human IgG detection limitation could be as low as 10 ng/mL.

3.2.2. Unclad/etched sensing structure

Unclad/etched sensing structure is made by removing part of fiber cladding, and then coating sensing region with metal film (Semwal et al., 2016; Li, L. et al., 2016a; Verma et al., 2018). Fig. 16 is the unclad/etched sensing structure.

When incident light propagating in core of optical fiber arrives at unclad region, part of light leaks out and forms evanescent wave. Surface plasmon resonance wave occurs with the appearance of evanescent wave. Assuming that the incident light angle is θ, the power in

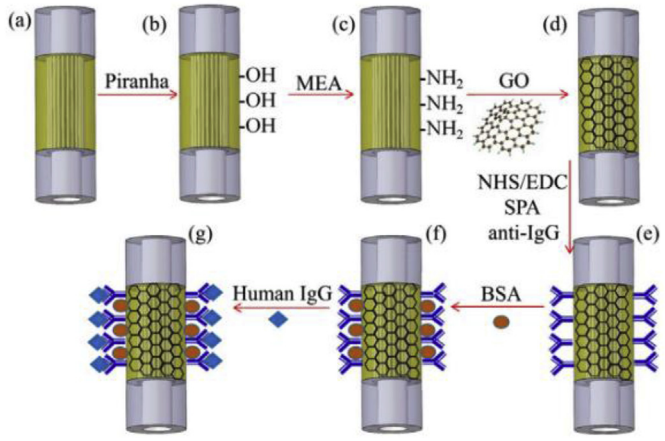

Fig. 14. The process for measuring immunoassay (Qi and Botao, 2018a).

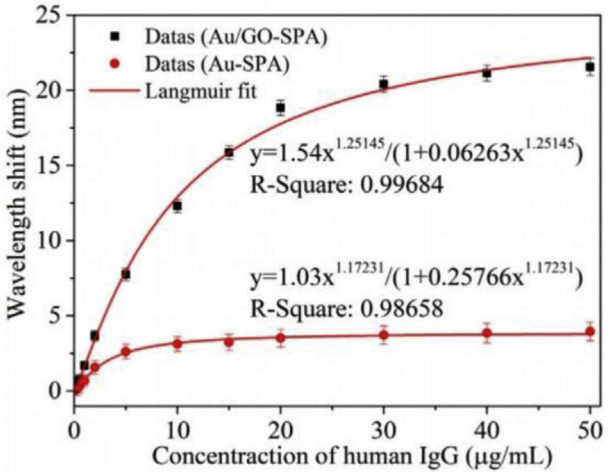

Fig. 15. Fitting curve between concentration of human IgG and wavelength shift (Qi and Botao, 2018a).

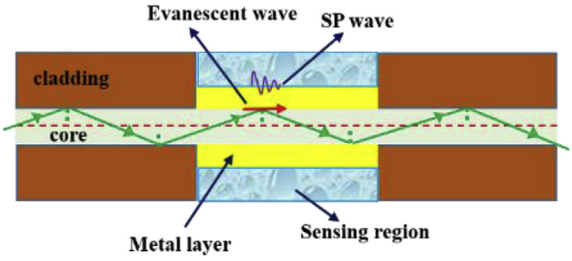

Fig. 16. Unclad/etched SPR sensing structure.

the end of output fiber is defined as dp, hence, dp can be described as (Mishra et al., 2016; Shushama et al., 2017):

$$dp \propto \mathrm{p}(\theta)d\theta \tag{7}$$

p(θ) is modal power, which is proportional to the incident light angle θ and can be described as:

$$\mathrm{p}(\theta) = \frac{n_c^2 \sin\theta\cos\theta}{(1 - n_c^2\cos^2\theta)^2} \tag{8}$$

Where n_c is refractive index of optical fiber core. According to reflective value, the normalized transmitted power of p-polarized light can be described as:

$$\mathrm{p}_{\mathrm{trans}} = \frac{\int_{\theta_{cr}}^{\frac{\pi}{2}} R_p^{Nref(\theta)}\mathrm{p}(\theta)\mathrm{d}\theta}{\int_{\theta_{cr}}^{\frac{\pi}{2}} \mathrm{p}(\theta)\mathrm{d}\theta} \tag{9}$$

Here, $Nref(\theta) = L/D\tan\theta$ represents the total reflected light in SPR sensor, L is the length of sensing region, D is the diameter of fiber core, θ_{cr} represents critical angle of total reflection in optic fiber and can be defined as:

$$\theta_{cr} = \sin^{-1}(n_{\mathrm{cl}}/n_c) \tag{10}$$

Where n_{cl} represents the refractive index of fiber cladding. The reflection is realized by four layer model analysis: fiber core, metal material, sensing layer and sensing medium, where fiber core is the first layer, metal material is the second layer and the complex dielectric function can be described by Lorentz-Drude formula. Here, the sensitive area of SPR sensor is generally far from light input fiber, hence, the polarization effect introduced by different launched rays can be neglected.

In optic fiber SPR sensor based on absorption, normalized transmitted power ($\mathrm{p}_{\mathrm{trans}}$) is affected by molar concentration (C) of the absorbing material. The transmitted power (δP_{trans}) altered with δC, and the sensitivity (S_c) of optic fiber SPR sensor based on absorption can be described as:

$$S_c = \left|\frac{\delta P_{trans}}{\delta C}\right| \tag{11}$$

In 2016, Shrivastav proposed a fiber optic sensor based on SPR with enzyme entrapped gel and silver film coated on fiber core, respectively (Shrivastav et al., 2016). Fig. 17 (a) was the sensing structure. The sensing principle was shown in Fig. 17 (b): ERY imprinted sites in the polymeric nanoparticle layer could combine with ERY molecules, which would affect the effective index of MIP nanoparticles. Experiment results shown in Fig. 17 (c) indicated that the sensitivity of proposed sensor was inversely proportional to the concentration of ERY. When the concentration of ERY was 0.01 μM, the sensitivity of proposed sensor got maximum and was 205 nm/μM.

3.2.3. D-shaped sensing structure

Unlike unclad/etched sensing structure, D-shaped sensing structure is made by removing partial cladding on one side of optical fiber, which can be seen in Fig. 18. In 2006, Wang firstly proposed a D-shaped optical fiber sensor based on SPR for refractive index sensing (Wang, S. F. et al., 2006). At present, most of side polished fiber sensors are made by SMF and MMF (Lo et al., 2011; Yue, 2013; Ubeid and Shabat, 2014). D-shaped sensing structure presents exciting advantages: easy fabrication, controllability of evanescent field, relatively higher robustness and so on (Lin, Y. C. et al., 2008; Patnaik et al., 2015). The sensing principle of D-shaped optical fiber sensor based on SPR can be expressed as:

When incident light enters into optical fiber at an angle θ_i less than critical angle, total reflection occurs, and the reflection coefficients of s-polarization and p-polarization can be described as (Cheng et al., 2000; Chen, K. H. et al., 2002):

$$r_{123}^t = \frac{r_{12}^t + r_{23}^t\exp(i2k_{z2}d_2)}{1 + r_{12}^t r_{23}^t\exp(i2k_{z2}d_2)} \tag{12}$$

Where $r_{ij}^t = (E_i^t - E_j^t)/(E_i^t + E_j^t)$, d_2 represents the thickness of metal material, and $t = p$, s, and

$$E_I^t = \begin{cases} n_j^2 k_{zi} & t = p \\ k_{zi} & t = s \end{cases}, \quad I = i, j, i \neq j, \quad i, j = 1,2,3 \tag{13}$$

Where k_{zi} represents wave vector component of medium i in z direction, and can be described as:

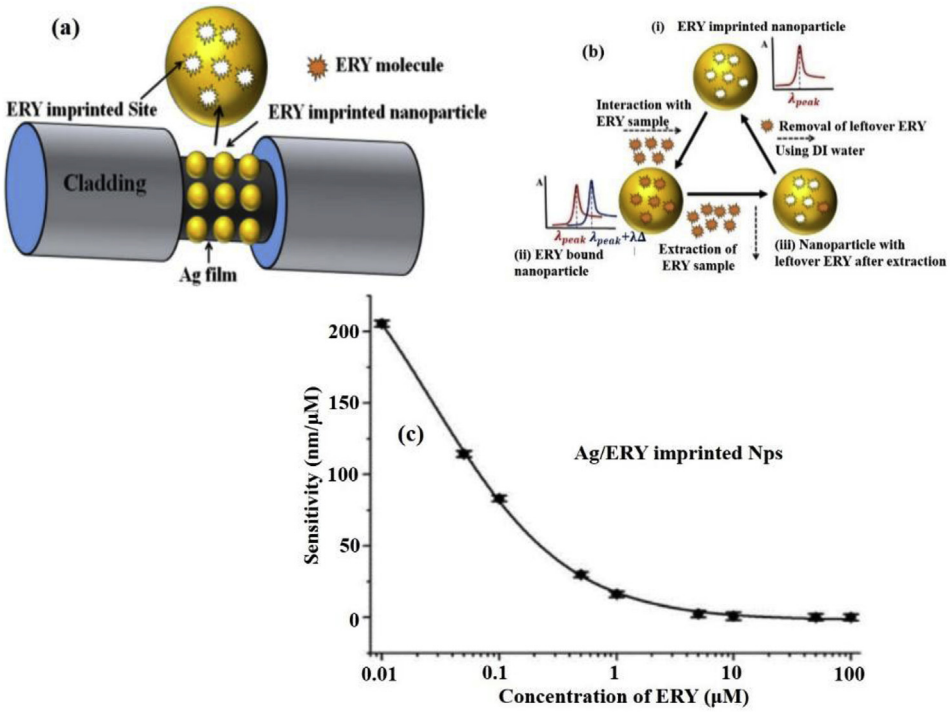

Fig. 17. (a) Sensing structure of proposed sensor, (b) sensing mechanism, (c) the relationship between concentration of ERY and sensitivity (Shrivastav et al., 2016).

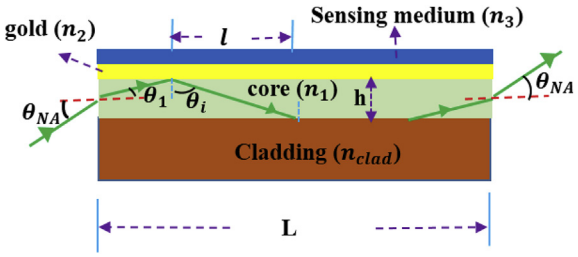

Fig. 18. The diagram of D-shaped optical fiber sensor based on SPR.

$$k_{zi} = k_0(n_i^2 - n_1^2 sin^2\theta_i)^{1/2} \tag{14}$$

Where k_0 is the wave vector in vacuum, and the amplitude reflection coefficients of r_{123}^p and r_{123}^s can be defined as:

$$r_{123}^p = |r_{123}^p| exp(i\varphi_p) \tag{15}$$

$$r_{123}^s = |r_{123}^s| exp(i\varphi_s) \tag{16}$$

Therefore, the phase difference (δ_i) between p-polarization and s-polarization components can be described as:

$$\delta_i = \varphi_p - \varphi_s \tag{17}$$

If length of sensing region in the D-shaped fiber biosensor is L, the height of the fiber core in the D-shaped structure is h. The variation of phase difference introduced by attenuated total reflection can be expressed as:

$$\varphi_{1,i} = m_i \delta_i \tag{18}$$

Where m_i presents the number of attenuated total reflections and can be described as:

$$m_i = \frac{L}{2h \tan\theta_i} \tag{19}$$

As the incident light with angle (θ_i) is at the input side of the sensing device, which will introduce phase-difference (δ_i') between p-polarization and s-polarization on account of the total internal reflection effect:

$$\delta_i' = 2\tan^{-1}\left\{\frac{[\sin^2\theta_i - (n_{clad}/n_l)^2]^{1/2}}{\tan\theta_i \sin\theta_i}\right\} \tag{20}$$

Where n_{clad} presents refractive index of fiber cladding, and the phase-difference introduce by total internal reflection can be expressed as:

$$\varphi_{2,i} = m_i' \delta_i' \tag{21}$$

Where m_i' presents the number of total internal reflection, numerically speaking, m_i' is equal to m_i, and the explanation is following: when incident angle is a fixed value, $\varphi_{2,i}$ is constant, and the total phase difference can be described as:

$$\varphi = \varphi_{1,i} + \varphi_{2,i} = m_i(\delta_i + \delta_i') \tag{22}$$

The existence of phase difference makes the spectrum change, thus D-shaped structure can be adopted for biomass sensing.

In 2016, Zhao, X. proposed a D-shaped optical fiber sensing probe based on SPR for avian influenza virus subtype H_6 sensing (Zhao, X. et al., 2016). A section of MMF with graded index was adopted for sensor, the core diameter and the thickness of cladding both were 62.5 μm. In order to get higher sensitivity, polished surface with special length, breadth and depth were designed, and they were 5 mm, 62.5 μm, and 62.5 μm, respectively. After side polished structure was completed, transferring gold film with the thickness of 40 nm on the surface of polished region. The diagram of the sensing probe is shown in Fig. 19.

Finally, EDC/NHS was covered on the film of gold to realize the measurement of avian influenza virus subtype H_6. For A/chicken/

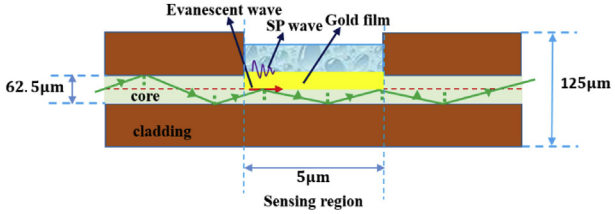

Fig. 19. Sensing structure of D-shaped optical fiber sensor.

Taiwan/2838V/00, experiment results revealed that the limitation of the proposed sensor was up to 5.14×10^5 EID_{50}/0.1 mL with 10 min average response time.

3.2.4. Tapered sensing structure

At present, most of the tapered fibers are made by stretching optical fiber along axial direction while heating optical fiber over a flame (Ding et al., 2017; Verma, 2018). With stretching, the diameter of optical fiber decreases gradually, and eventually, the part of light in fiber core leaks out of optical fiber to excite SPR (María-Cruz et al., 2014; Al-Qazwini et al., 2015; Goswami et al., 2016).

In tapered optical fiber sensing probe, the diameter of tapered optical fiber is usually several microns, and after incident light entering into tapered region, the angle of ray decreases gradually, and approaches critical angle of total reflection, where part of incident light leaks into optical fiber cladding. After coating tapered region with metal material, the evanescent field maximize coupling between surface plasmon wave and the evanescent, hence, the spectral intensity of tapered sensor can be improved. After decades of development, tapered sensing probe has been applied in optical fiber sensor due to its ability to enhance the sensitivity (Natalia et al., 2011; Cennamo et al., 2014).

The sensing structure of tapered fiber optic sensor based on SPR is presented in Fig. 20, and the sensing principle can be explained as (Verma et al., 2008):

When incident light enters into the tapered region, transmitted light will be refracted and reflected. Refractive index and dielectric constant of the tapered region covered with metal material are defined as n_s and ε_m, ε_m can be expressed as:

$$\varepsilon_m(\lambda) = \varepsilon_{mr} + i\varepsilon_{mi} = 1 - \frac{\lambda^2\lambda_c}{\lambda_p^2(\lambda_c + i\lambda)} \tag{23}$$

Where λ_p and λ_c represent collision wavelength and the plasma wavelength, respectively, which are determined by coated material, for gold material, λ_p and λ_c are 1.6826×10^{-7} m and 8.9342×10^{-6} m (Ordal et al., 1983), respectively.

If the following condition is satisfied, SPR occurs.

$$\frac{2\pi}{\lambda} n_1 \sin\theta = \mathrm{Re}\left[\frac{2\pi}{\lambda}\left(\frac{\varepsilon_m n_s^2}{\varepsilon_m + n_s^2}\right)^{1/2}\right] \tag{24}$$

Where n_1 represents refractive index of fiber core. The right side of equation (24) is real part of surface plasmon propagation constant (K_{sp}). In tapered fiber sensor based on SPR, sensitivity is characterized by wavelength, therefore, set the incident angle to a fixed value. According to analysis, it is obvious that resonance wavelength (λ_{res}) is affected by refractive index (n_s) of environment. If δn_s is the change of refractive index, then the change of resonance wavelength shifts can be described as $\delta\lambda_{res}$. Hence, the sensitivity (S_n) of tapered fiber sensor based on SPR can be defined as:

$$S_n = \frac{\delta\lambda_{res}}{\delta n_s} \tag{25}$$

Where λ_{res} is the resonance wavelength of tapered optical fiber sensor based on SPR.

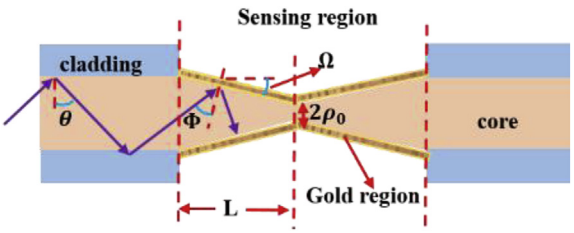

Fig. 20. Schematic diagram of proposed tapered optical fiber sensor based on SPR.

During the past few years, many tapered optical fiber sensor based on SPR have been proposed, and the sensitivity of tapered probe could be up to 12000 nm/RIU by enhancing the interaction of propagating modes with metallic coating (Óscar et al., 2011). In order to realize the measurement of biomass or chemical content, some intermediaries should be adhered on sensing region. However, the fragility of tapered probe restricts the application of it on biometric.

3.2.5. U-shaped sensing structure

Compared with tapered sensing structure, the evanescent field of the U-shaped sensing structure can be enhanced by bending the fiber optic in sensing region, which makes it popular in SPR based fiber optic sensor to increase sensitivity (Sai et al., 2009; Zhang, C. et al., 2017; Ariadny et al., 2018).

When the incidence light propagates in a U-shaped optical fiber, all light rays will be reflected at the core-cladding interface, and total reflection occurs when the incident angle is larger than critical angle which defined as:

$$\theta_c = \sin^{-1}\left(\frac{n_{cl}}{n_{co}}\right) \tag{26}$$

Where n_{cl} presents refractive index of fiber cladding and n_{co} presents refractive of fiber core. When the propagation angle is greater than θ_c, some light leaks into optical fiber cladding. What's more, the amount of lost modes are positively correlated with outside medium refractive index. For U-shaped sensor based on SPR, the light leaks to the external medium means the enhancement of the evanescent field, which is more conducive to the realization of SPR, and the resonance spectrum will be more sensitive to refractive index of medium changing. In addition, the change of measured biomass will cause the change of refractive index. Therefore, the U-shaped fiber sensors based on SPR can be adopted for measurement of biomasses.

In 2017, Zhang proposed a U-shaped plastic optic fiber sensor based on SPR for detection of aqueous glucose (Zhang, C. et al., 2017). The sensing structure was made by plastic optic fiber with the length of 30 cm, and then the plastic optic fiber was put in a manual device to form a U-shaped structure with inner diameter of 1 mm, after which the laser-induced deposition of the AgNPs and the dip-coating of graphene were executed (as shown in Fig. 21). Experiment results revealed that the shifts for the resonance wavelength were respectively up to 32 and 16 nm for the 90% aqueous ethanol and 20% aqueous glucose, corresponding refractive index (RI) 1.3657 and 1.3557. These results implied that this graphene/AgNPs U-bent fiber optic SPR sensor would provide a promising method for the detection in the field of medicine, biotechnology and food safety.

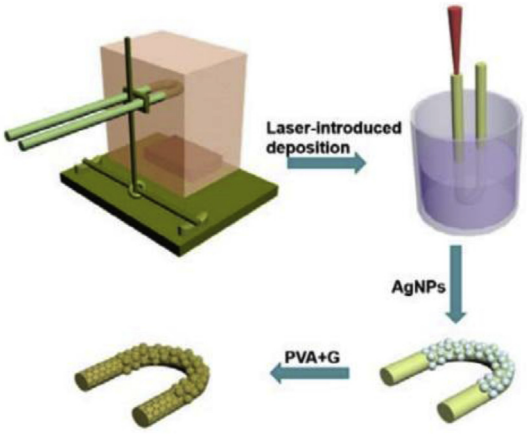

Fig. 21. The making process of U-bend plastic optic fiber sensor based on SPR (Zhang et al., 2017a,b).

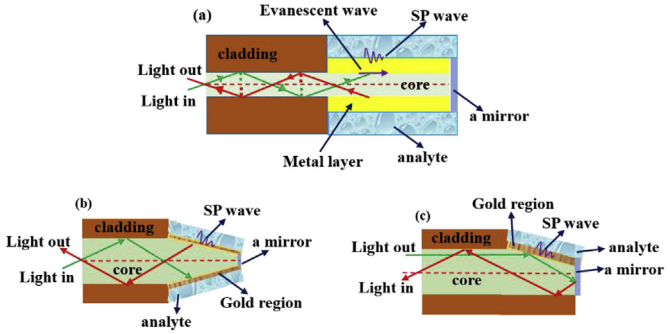

Fig. 22. The diagram of end-surface optical fiber sensor. (a) flat tip, (b) tapered tip, (c) angle polished tip.

3.2.6. End-face reflected sensing structure

The sensing structures introduced above are all transmission. Compared with transmission-based optical fiber sensor, the end-surface reflected sensing device is more convenient to insert into measured object (Yanase, 2010; Sannomiya, 2013; Zhao, C. et al., 2017). At present, there are two types of end-surface sensor probes: flatness of reflective end surface (shown in Fig. 22 (a)) and inclination of reflective end surface (shown in Fig. 22 (b) and (c)). At the end of the optic fiber, the cladding is removed and coated with metal material to generate SPR effect. Moreover, when incident light passes through reflected interface to the incident point of light, the optical path doubles, which increases the resonance effect and produces more effective sensing area.

After decades of development, end-face reflected sensor has developed well in bio-sensing field. In 2015, Se proposed a fiber optic sensor based on SPR for immunoassays detection (Se et al., 2015). And then the sensing region covered with gold film with the thickness approximately 56.3 nm. The fabrication process of ELP and modification process of PDA for immunoassay were shown in Fig. 23.

The scanning electron microscopy (SEM) after gold plating was shown in Fig. 24. After transferring goat anti-human IgG antibodies on the surface of polydopamine-modified gold film, the resonance wavelength shifted 66.21 nm. What's more, the LOD of the proposed sensor was low to 2 μg/mL with the sensitivity of 0.41 nm per μg/mL, where the sensitivity and LOD of the proposed sensor were about four times and seven times than that of mercaptoundecanoic acid-modified gold film surface to human IgG, respectively.

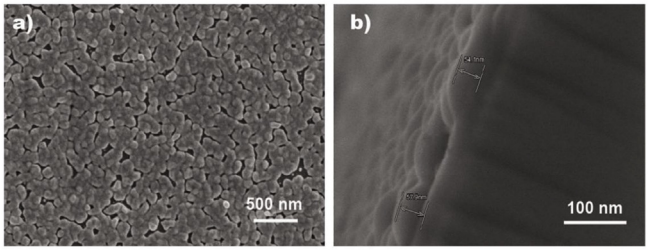

Fig. 24. (a) SEM images of the surface cross-section (b) SEM images of gold film (Se et al., 2015).

3.3. Comparison of different sensing structure

From the above analyses, it is clear that many efforts have been made to develop optical fiber biosensor based on SPR, and have been adopted for detection of DNA, living cells, proteins, viruses, bacteria, glucose, and so on (Li et al., 2015; Wu, J. et al., 2015; Chen, Y. et al., 2015; Christina et al., 2018). Detection of biomass mainly depends on the combination of analyte target and corresponding biological recognition element. In addition, response time, sensitivity and measurement range of these biomass mainly depend on their corresponding bio-sensitive membranes. Hence, different sensing structures have no comparability in response time, sensitivity and measurement range. While, the inherent characteristics of different sensing structure are compared, which is presented in Table 1.

As shown in Table 1, the first six sensing structures are transmission sensing structure and the last one is reflection sensing structure. Different sensing structures have their merit and demerit. Optical fiber grating is a moderation choice. Hetero-core sensing structure is relatively simple making, the structure is stable and economical. Unclad/etched sensing structure is mainly made by corrosion method to remove optical fiber cladding, the reducing of penetration depth of evanescent wave can make evanescent wave reach the measurement quickly, and improve the sensitivity of measurement. However, the reduction of diameter of sensing area makes it fragile. For D-shaped sensing structure, although sensitivity is inferior, the mechanical strength is merit. While for tapered sensing structure, the diameter of fiber core and cladding reduced simultaneously. However, the sensing structure is gotten by stretching optical fiber, which makes the length of sensing

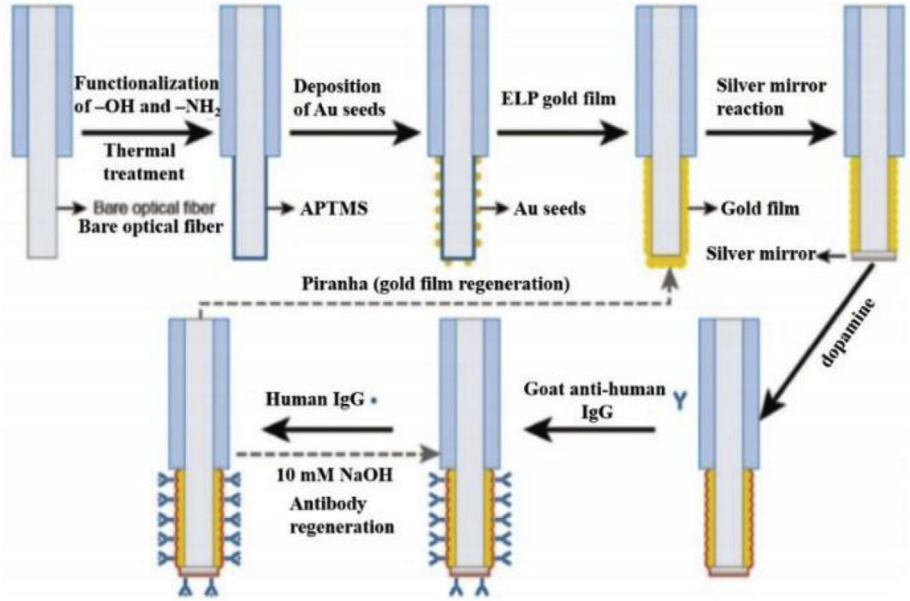

Fig. 23. The sensor making process (Se et al., 2015).

Table 1
Comparison of different fiber optic coupled biosensor based on SPR.

performance	Optical fiber grating	Hetero-core structure	Unclad/etched fiber	D-shaped fiber	Tapered fiber	U-shaped fiber	End face reflect
Sensor cost	low	Relatively low	low	Relatively high	high	low	moderate
Sensor size	moderate	moderate	moderate	moderate	large	Relatively large	small
Fabrication difficulty	Relatively high	Relatively low	high	Relatively high	Relatively high	low	Relatively high
Mechanical strength	Relatively high	Low	simple	High	Relatively high	Low	Relatively high

region increase. And for U-shaped fiber optic sensor based on SPR, the bulk of U-shaped structure is largest, which limits it in practical application in narrow environment. Moreover, end-face reflected sensing structure, the incident and output of light are at the same end, the incident and output of light are the same end, but the metal film coating progress may increase the difficulty of the fabrication process.

Generally speaking, each has its own advantages. In practical applications, the corresponding sensing structures can be adopted according to requirement.

4. Recent development

Practicality is the ultimate goal of any scientific research. While in practical application, many kinds of biomass exist, so it is necessary to realize the simultaneous measurement of multiple biomass, which is also of great concern in recent years. Moreover, high sensitivity has always been the goal of sensor researchers, and the emergence of nanomaterial brings alluring prospect.

4.1. Optical fiber biosensor based on SPR for multi-parameters detection

In practical applications, simultaneous detection of multi-parameter is research hotpot in optical fiber biosensor based on SPR (Lin et al., 2012; Li et al., 2016b). At present, multiple parameters detection sensor is made by made by compacting different sensing regions on a single fiber optic sensing probe. While, how to distinguish the spectrum corresponding to each sensing region is the key for multiple parameters detection, and prospective methods are following: firstly, covering sensing regions with different metal films, for instance, gold and silver films have different surface plasmon resonance positions. Secondly, covering a metal film with different thickness in different sensing regions. Thirdly, coating the same thickness of metal film in the sensing area, and then covering different high refractive index material on sensing regions. However, controlling film thickness is difficult. Lastly, adjusting the incident angle of resonance wave is an effective method.

For instance, in 2016, Tabassum proposed a sensor for simultaneous measurement of two parameters, the sensor was made by cascading two optical fiber sensors based on SPR together and adopted for the measurement of VK_1 and heparin (Tabassum and Gupa, 2016). The sensing structure was seen in Fig. 25 (a), where two parts of cladding were removed on the optical fiber. The valley position of SPR resonance effect was different due to the excitation of different metal films. Therefore, one part was covered with nanohybrid of multiwalled carbon nanotube in chitosan on the surface of silver film and adopted for VK_1 measurement, and the other part was covered with ZnO and polybrene on the surface of copper adopted for heparin measurement. The experiments results were shown in Fig. 25 (b), which indicated that the spectrum shifted to long wavelength direction with the concentration of heparin and VK_1 from 0 to 10^{-3} ug/l. What's more, the LODs of the proposed sensor for heparin and VK_1 are 2.88×10^{-4} mg/l and 2.66×10^{-4} mg/l, respectively. Such multi-parameters detection method has been proved for clinical analyses and fulfill the need for simultaneous detection of multiple parameters.

4.2. Nanomaterial applied in optical fiber sensor based on SPR

Sensitivity is an issue that biosensors must consider. Nanomaterial includes nanoparticles, nanomembranes, nanorods, nanoflowers and nanofibers, and possess higher surface of volume ratio (or the aspect ratio) that enables an effective interaction of analyte molecules with the entities on the sensing surface in comparison with bulk layers. Small dimensions and unique physical properties combined with strong plasmonic response are attractive and enable nanomaterial can be adopted to improve sensor sensitivity (Kant et al., 2018). Antohe has proved that the sensitivity improved 25% compared with the non-patterned counterparts by covering periodic triangular gold nanoparticles on the surface of optic fiber sensor based on SPR (Antohe et al., 2017). In addition, the special functional groups on nanomaterial make it better selectivity to biomass, which can improving the measurement accuracy of sensors.

5. Conclusion and future prospects

This current paper minutely summarizes recent contemporary research in the spectacular and highly promising field of optical fiber biosensor based on SPR. Four implementation strategies to generate SPR are systematically introduced, and optical fiber coupling sensing structure has merit compared with other three devices and finally adopted for biosensor. A comprehensive and mainstream classification of optical fiber biosensor based on SPR is presented: optical fiber grating biosensor based on SPR and optical fiber structured type biosensor based on SPR. Each sensing structure has its own merits, befitting sensing structure can be selected in practical application. Instances consummately verify optical fiber sensor based on SPR has been

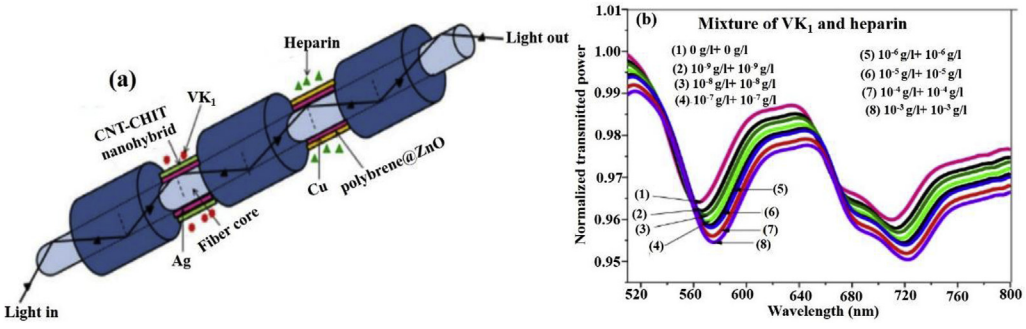

Fig. 25. (a) The sensing structure of proposed sensor, (b) the experiment spectrum (Tabassum and Gupa, 2016).

extensively applied in biosensing and has very wide popularization and application prospects, while, existing optical fiber biosensors based on SPR are only applied in laboratory environments at present, commercial application successful is one challenge and should be one of the future goal. Moreover, detection of multiple parameters and sensitivity improvement are now compared, while, subsistent optical fiber biosensor based on SPR is two-parameter, the ability to detect multiple parameters within one optical fiber device is another challenge for biosensor. Although sensitivity is satisfactory, response time and reuse of sensor are lack of concern. Come what may, starting from academic interests and innovative development ideas, hoping efficient optical fiber biosensor based on SPR invokes the readers towards an unabridged understanding and appreciation.

Declaration of interest statement

There are no interests to declare.Acknowledgements

This work was supported in part by the National Natural Science Foundation of China under Grant 61425003 and 61773102, the Fundamental Research Funds for the Central Universities under Grant N160408001, N170407005 and part by the State Key Laboratory of Synthetical Automation for Process Industries under Grant 2013ZCX09.

Conflict of interest

There is no Conflict of interest.

References

Al-Qazwini, Y., Noor, A.S.M., Yaacob, M.H., Harun, S.W., Mahdi, M.A., 2015. Sensors & Actuators A Physical. 236, 38–43.
An, G., Li, S., Qin, W., Zhang, W., Fan, Z., Bao, Y., 2014. Plasmonics 9, 1355–1360.
Antohe, I., Spasic, D., Delport, F., Li, J., Lammertyn, J., 2017. Nanotechnology 28, 215301.
Arasu, P.T., Noor, A.S.M., Shabaneh, A.A., Yaacob, M.H., Lim, H.N., Mahdi, M.A., 2016. Opt. Commun. 380, 260–266.
Ariadny, A., Dutra, Fábio, Regina, A., Werneck, M., 2018. Sensors 18, 648–663.
Bhatia, V., Vengsarkar, A.M., 1996. Opt. Lett. 21, 692–694.
Boruah, B.S., Biswas, R., 2018. Opt. Fiber Technol. 46, 152–156.
Caucheteur, C., Guo, T., Albert, J., 2015. Anal. Bioanal. Chem. 407, 3883–3897.
Cennamo, N., D'Agostino, G., Pesavento, M., Zeni, L., 2014. Sens. Actuators B Chem. 191, 529–536.
Chen, K.H., Hsu, C.C., Su, D.C., 2002. Opt. Commun. 209, 167–172.
Chen, Y., Yu, Y., Li, X., Zhou, H., Hong, X., Geng, Y., 2015. Sens. Actuators B Chem. 226, 412–418.
Cheng, Y.C., Su, W.K., Liou, J.H., 2000. Opt. Eng. 39, 311–314.
Chong, J.H., Shum, P., Haryono, H., Yohana, A., Rao, M.K., Lu, C., Yinian, Z., 2004. Opt. Commun. 229, 65–69.
Christina, G.D., Subrahmanyam, A., Sai, V.V.R., 2018. Raman spectroscopy 49, 1607–1616.
Chryssis, A.N., Lee, S.M., Lee, S.B., Saini, S.S., Dagenais, M., 2005. IEEE Photonics Technol. Lett. 17, 1253–1255.
Dai, Y., Xu, H., Wang, H., Lu, Y., Wang, P., 2018. Opt. Commun. 416, 66–70.
Ding, Z.W., Lang, T.T., Wang, Y., Zhao, C.L., 2017. J. Light. Technol. 35 1-1.
Goswami, N., Chauhan, K.K., Saha, A., 2016. Opt. Commun. 379, 6–12.
Guo, X., 2012. Biophotonics 5, 483–501.
Guo, T., Han, L., Xie, C., Xu, P., Lao, J., Zhang, X., Xu, J., Chen, X., Huang, Y., Liang, X., Mao, W., Guan, B., 2016a. J. Light. Technol. 99 1-1.
Guo, T., Liu, F., Guan, B.O., Albert, J., 2016b. Opt. Laser. Technol. 78, 19–33.
Gupta, B.D., Kant, R., 2018. Opt. Laser. Technol. 101, 144–161.
Heather, J.P., Alan, D.K., Frank, B., 1998. Journal of Lightwave Technoloty 16, 1606–1612.
Hill, K.O., Fujii, Y., Johnson, D.C., Kawasaki, B.S., 2008. Appl. Phys. Lett. 32, 647–649.
Hosoki, A., Nishiyama, M., Igawa, H., Seki, A., Choi, Y., Watanabe, K., 2013. Sens. Actuators B Chem. 185, 53–58.
Hu, W., Huang, Y., Chen, C., Liu, Y., Guo, T., Guan, B.O., 2018. Sens. Actuators B Chem. 264, 440–447.
Iadicicco, A., Cusano, A., Cutolo, A., Bernini, R., Giordano, M., 2004. IEEE Photonics Technol. Lett. 16, 1149–1151.
Ji, M., Xu, M., Zhang, W., Yang, Z., Huang, L., Liu, J., Zhang, Y., Gu, L., Yu, Y., Hao, W., An, P., Zheng, L., Zhu, H., Zhang, J., 2016. Adv. Mater. 28, 3094–3101.
Jorgenson, R.C., Yee, S.S., 1993. Sens. Actuators B 12, 213–220.
Jorgenson, R. C., 1993. Washington: University of Washington. 8992: 89920A-89920A-8.
Kang, Y.Y., Wang, Y.J., Yang, L.K., Wang, Y.T., 2011. Appl. Mech. Mater. 128, 580–583.
Kant, R., Tabassum, R., Gupta, B.D., 2018. Biosens. Bioelectron. 99, 637–645.
Kao, K.C., Hockham, G.A., 1966. Proc. Inst. Electr. Eng. 113, 1151–1158.
Kretschmann, E., Raether, H., 1968. Z. Naturforschung 23, 2135–2136.
Kretschmann, E., 1971. Z.Physik. 241, 313–324.
Laffont, G., Ferdinand, P., 2001. Meas. Sci. Technol. 12, 765–770.
Lee, B., Roh, S., Park, J., 2009. Opt. Fiber Technol. 15, 209–221.
Li, D., Wu, J., Wu, P., Lin, Y., Sun, Y., Zhu, R., Jia, Y., Kexin, X., 2015. Sens. Actuators B Chem. 213, 295–304.
Li, L., Liang, Y., Liu, Q., Peng, W., 2016a. IEEE Photonics Technol. Lett. 28 1-1.
Li, L., Zhang, X., Liang, Y., Guang, J., Peng, W., 2016b. J. Biomed. Opt. 21 (12), 127001.
Liedberg, B., Nylander, C., Ingemar, Lunström, 1983. Sens. Actuators 4, 299–304.
Liedberg, B., LundstroM, I., Stenberg, E., 1993. Sens. Actuators B 11, 63–72.
Lin, H.Y., Huang, C.H., Huang, C.C., Liu, Y.C., Chau, L.K., 2012. Opt. Lett. 37, 3969–3971.
Lin, Y.C., Tsao, Y.C., Tsai, W.H., Hung, T.S., Chen, K.S., Liao, S.C., 2008. Sensors and Actuators B (Chemical) 133, 370–373.
Liu, L., Yang, J., Yang, Z., Wan, X., Hu, N., Zheng, X., 2013. Sensors 13, 7443–7453.
Liu, X., Zhang, X., Cong, J., Xu, J., Chen, K., 2003. Sens. Actuators B 96, 468–472.
Liu, Z., Liu, L., Zhu, Z., Zhang, Y., Wei, Y., Zhang, Y., Yang, J., Yuan, L., 2017. Opt. Commun. 403, 290–295.
Lo, Y.L., Chuang, C.H., Lin, Z.W., 2011. Opt. Lett. 36, 2489–2491.
Luo, B., Yan, Z., Sun, Z., Liu, Y., Zhao, M., Zhang, L., 2015. Opt. Express 23, 32429–32440.
Lyons, E.R., Lee, H.P., 1999. Photonics Technology Letters 11, 1626–1628.
María-Cruz, Navarrete, Natalia, Díaz-Herrera, Agustín, González-Cano, óscar, Esteban, 2014. Sens. Actuators B Chem. 190, 881–885.
Marques, L., Hernandez, F.U., James, S.W., Morgan, S.P., Clark, M., Tatam, R.P., 2016. Biosens. Bioelectron. 75, 222–231.
Meltz, G., Morey, W.W., Glenn, W.H., 1989. Opt. Lett. 14, 823–825.
Meltz, G., Morey, W.W., Glenn, W.H., 1990. Tech. dig.opt.Optical Fiber Commun. Conf. (san Francisco Jan).
Mishra, S.K., Bhardwaj, S., Dhar Gupta, B., 2015. Sensors Journal IEEE 152, 1235–1239.
Mishra, A.K., Mishra, S.K., Verma, R.K., 2016. G The Journal of Physical Chemistry C 120, 2893–2900.
Natalia, Díaz Herrera, óscar, Esteban, María-Cruz, Navarrete, Agustín, González-Cano, Orellana, G, B.P.E., 2011. Opt. Lasers Eng. 49, 1065–1068.
Ordal, M.A., Long, L.L., Bell, R.J., Bell, S.E., Bell, R.R., 1983. Appl. Opt. 22, 1099–1119.
Óscar, E., Naranjo, F.B., Natalia, Díaz-Herrera, Valdueza-Felip, S., Agustín, González-Cano, 2011. Sens. Actuators B Chem. 158, 372–376.
Otto, A., 1968. Zeitschrift für Physik. 216, 398–410.
Patnaik, A., Senthilnathan, K., Jha, R., 2015. IEEE Photonics Technol. Lett. 27, 2437–2440.
Patrick, H.J., Chang, C.C., Vohra, S.T., 1998. Electron. Lett. 34, 1773–1775.
Perlette, J., Tan, W., 2001. Anal. Chem. 73, 5544–5550.
Qi, W., Botao, W., 2018a. Opt. Laser. Technol. 107, 210–215.
Ritchie, R.H., 1957. Phys. Rev. 106, 874–881.
Ruijie, T., Yong, Z., Maoqing, C., Yun, P., 2018. Sens. Actuators 280, 24–30.
Sai, V.V.R., Kundu, T., Mukherji, S., 2009. Biosens. Bioelectron. 24, 2804–2809.
Sannomiya, T., 2013. Sens. Actuators B Chem. 181, 611–619.
Schasfoort, R.B.M., Tudos, A.J., 2008. The Royal Society of Chemistry, Cambridge, UK.
Se, S., Libing, W., Rongxin, X., Boshi, L., Renliang, H., Wei, Q., Zhimin, H., 2015. Biosens. Bioelectron. 74, 454–460.
Semwal, V., Shrivastav, A.M., Verma, R., Gupta, B.D., 2016. Sens. Actuators B Chem. 230, 485–492.
Sergiy, Patskovsky, Kabashin, Andrei V., Meunier, Michel, 2003. Proc. SPIE-Int. Soc. Opt. Eng. 4958, 144–148.
Sharma, A.K., Jha, R., Gupta, B.D., 2007. IEEE Sens. J. 7, 1118–1129.
Shevchenko, Y.Y., Albert, J., 2007. Opt. Lett. 32, 211–213.
Shevchenko, Y., Francis, T.J., Blair, D.A.D., Walsh, R., Albert, J., 2011. Anal. Chem. 83, 7027–7034.
Shi, S., Wang, L., Wang, A., Huang, R., Ding, L., Su, R., Qi, wei, He, Zhimin, 2016. J. Mater. Chem. C. 4, 7554–7562.
Shrivastav, A.M., Mishra, S.K., Gupta, B.D., 2015. Sens. Actuators B Chem. 212, 404–410.
Shrivastav, A.M., Usha, S.P., Gupta, B.D., 2016. Biosens. Bioelectron. 90, 516–524.
Shushama, K.N., Rana, M.M., Inum, R., Hossain, M.B., 2017. Opt. Commun. 383, 186–190.
Sipe, J.E., Erdogan, T., 1996. J. Opt. Soc. Am. A 13, 296–313.
SlaviK, R., Homola, J., Brynda, E., 2002. Biosens. Bioelectron. 17, 591–595.
Srivastava, S.K., Arora, V., Sapra, S., Gupta, B.D., 2012. Plasmonics 7, 261–268.
Srivastava, S.K., Verma, R., Gupta, B.D., 2016. Opt. Commun. 369, 131–137.
Tabassum, R., Gupta, B.D., 2016. Biosens. Bioelectron. 86, 48–55.
Takagi, K., Sasaki, H., Seki, A., Watanabe, K., 2010. Sens. Actuators A Phys. 161, 1–5.
Tu, G., Deogratias, N., Meng, X., Li, X., Liu, J., Lan, J., Jiang, L., Yang, Y., Zhang, J., 2018. Materials Chemistry Frontiers 2, 1720–1724.
Tsuda, H., Urabe, K., 2009. Sensors 9, 4559–4571.
Ubeid, M.F., Shabat, M.M., 2014. Opto-Electron. Rev. 22, 191–195.
Updike, S.J., Hicks, G.P., 1967. Nature 214, 986–988.
Valérie, Voisin, Pilate, J., Damman, P., Patrice, Mégret, Caucheteur, C., 2014. Biosens. Bioelectron. 51, 249–254.
Vengsarkar, A.M., Lemaire, P.J., Judkins, J.B., Bhatia, V., Erdogan, T., Sipe, J.E., 1996a. J. Light. Technol. 41, 58–65.
Vengsarkar, A.M., Pedrazzani, J.R., Judkins, J.B., Lemaire, P.J., Davidson, C.R., 1996b. Opt. Lett. 21, 336–338.
Verma, R.K., Sharma, A.K., Gupta, B.D., 2008. Opt. Commun. 281, 1486–1491.
Verma, R.K., Suwalka, P., Yadav, J., 2018. Opt. Fiber Technol. 43, 95–100.
Verma, R.K., 2018. Optik - International Journal for Light and Electron Optics 108, 330–343.
Wada, A., Tanaka, S., Takahashi, N., 2012. IEEE Sens. J. 12, 225–229.
Wang, H.Z., Gao, Y.Y., Liu, J., Li, M.W., Ji, E., Zhang, X.Y., Cheng, M., Xu, J.J., Liu, H.P.R., Chen, W.X., Fan, F.T., Li, C., Zhang, J.T., 2019. Adv. Energy Mater. https://

doi.org/10.1002/aenm.201803889.
Wang, S.F., Chiu, M.H., Chang, R.S., 2006. Sens. Actuators B Chem. 114, 120–126.
Wang, M., Li, H., Xu, T., Yu, M., Xu, J., 2018. J. Light. Technol. 36, 5927–5934.
Weis, R.S., Kersey, A.D., Berkoff, T.A., 1994. IEEE Photonics Technol. Lett. 612, 1469–1472.
Wijaya, E., Cédric, Lenaerts, Maricot, S., Hastanin, J., Habraken, S., Vilcot, J.P., Boukherroub, R., Szunerits, S., 2011. Curr. Opin. Solid State Mater. Sci. 15, 0–224.
Wong, W.C., Chan, C.C., Boo, J.L., Teo, Z.Y., Tou, Z.Q., Yang, H.B., Li, C., Leong, K.C., 2013. IEEE J. Sel. Top. Quantum Electron. 19 4602107-4602107.
Wu, J., Yan, Y., Li, S., Ding, X., 2015. Meas. Sci. Technol. 26 (1–7), 105701.
Xu, M., Tu, G., Ji, M., Wan, X., Liu, J., Liu, J., Rong, H., Yang, Y., Wang, C., Zhang, J., 2019. DOI: 10.1007/s12274-019-2325-8.
Yanase, Y., 2010. Biosens. Bioelectron. 25, 1244–1247.
Yong, Z., Maoqing, C., Riqing, L., Feng, X., Anning, S., 2018a. Sens. Actuators A Phys. 270, 162–169.
Yong, Z., Qilu, W., Yanan, Z., 2018b. Sens. Actuators B Chem. 258, 822–828.
Yong, Z., Ruijie, T., Maoqing, C., Feng, X., 2019. Sens. Actuators B Chem. 284, 96–102.
Yu, Q., Yong, Z., Qilu, W., Yang, Y., 2018. Sens. Actuators B Chem. 260, 86–105.
Yue, J.H., 2013. Opt. Express 21, 23498–23510.
Zainuddin, N.H., Fen, Y.W., Alwahib, A.A., Yaacob, M.H., Bidin, N., Omar, N.A.S., 2018. Optik 168, 134–139.
Zhang, C., Li, Z., Jiang, S.Z., Li, C.H., Man, B.Y., 2017a. Sens. Actuators B Chem. 251, 127–133.
Zhang, J., Tang, X., Dong, J., Wei, T., Xiao, H., 2009. Sens. Actuators B Chem. 1352, 420–425.
Zhang, Y., Shoaib, A., Li, J., Ji, M., Wei, Q., 2016. Biosens. Bioelectron. 79, 866–873.
Zhang, Y., Wang, F., Qian, S., Liu, Z., Wang, Q., Gu, Y., Wu, Z., Jing, Z., Sun, C., Peng, W., 2017b. Sensors 17, 2259–2267.
Zhang, Y.N., Zhao, Y., Zhou, T., Wu, Q.L., 2018. Lab Chip 18, 57–74.
Zhao, C., Wan, Y., Wan, D., Din, Z., 2017. Photonic Sensors 7, 105–112.
Zhao, X., Tsao, Y.C., Lee, F.J., Tsai, W.H., Wang, C.H., Chuang, T.L., Wu, M.S., Lin, C.W., 2016. J. Virol Methods 233, 15–22.